Silkworm Silk under Tensile Strain Investigated by Synchrotron X-ray Diffraction and Neutron Spectroscopy

Tilo Seydel,*,† Klaas Kölln,‡ Igor Krasnov,‡ Imke Diddens,‡ Nadine Hauptmann,‡ Gesa Helms,‡ Malte Ogurreck,‡ Shin-Gyu Kang,†,‡ Michael M. Koza,† and Martin Müller‡

Institut Laue-Langevin, B.P. 156, F-38042 Grenoble, France, and IEAP, University of Kiel, Olshausenstrasse 40, D-24098 Kiel, Germany

Received October 20, 2006; Revised Manuscript Received December 14, 2006

ABSTRACT: The molecular structure of *Bombyx mori* silkworm silk fibers is investigated in situ upon externally applied tensile stress using synchrotron X-ray diffraction, while the molecular vibrational response is investigated using cold neutron time-of-flight spectroscopy. The aligned silk fibers are therefore exposed to a tensile force along the fiber axis generated by stretching machines adapted to X-ray and neutron scattering, respectively, and the stress−strain curves are measured in situ. The applied force in both cases is sufficient to reach the yield point of plastic deformation. In the case of neutron spectroscopy, different regions within the hierarchical silk structure are masked by selective deuteration. The X-ray studies confirm the assumption that most of the deformation upon extension of the fibers is due to the amorphous regions of the silk. The neutron results indicate that the externally applied force is not reflected by any noticeable effect on the molecular vibrational or diffusional/reorientational level in the range accessible to neutron time-of-flight spectroscopy. This observation of unaffected molecular dynamics is in agreement with a model of entropy elasticity.

1. Introduction

Considerable interest has since long arisen in mimicking biological high-performance polymers for their extraordinary mechanical properties. Silk fibers, among them those with the most outstanding mechanical properties such as spider dragline, consist of a protein polymer composite structure made out of crystalline and amorphous regions (see, e.g., refs 1−3 and references therein). Experimental results from various techniques studying the morphology of silks, such as NMR, X-ray diffraction, and infrared spectroscopy, have been reported in the literature (see, e.g., refs 4 and 5). The research interest, although predominantly focused on the most fascinating spider silk fibers, also includes the chemically and mechanically similar and more abundant silkworm silk fibers.[6] While spider and silkworm silks and their various subtypes differ considerably in the details of sequence and structure, a combination of crystallites and an amorphous polymer matrix—however, with strongly varying volume fractions—seems to be common to all silks (for a comparative study, see, e.g., ref 7 and references therein). The natural variability in the details of the supramolecular structure of silks is reflected by a corresponding variability of the mechanical properties, which also depend on details of the spinning process such as the extrusion or reeling speed.[8] Remarkably, the mechanical properties of silkworm silk can approach those of spider silk under optimized harvesting conditions.[8] According to a morphological model of spider silk, small crystalline blocks are surrounded by a matrix containing both oriented and unoriented amorphous material.[9] Although the amino acid sequences and supramolecular composition of the silk protein polymer chains are being unravelled[10] and models for the mechanical properties are being discussed,[11] our understanding of the link between the hierarchical structure and function remains limited. It seems probable that the protein polymeric chains within the amorphous regions contribute—on a molecular level—to the mechanical properties.[12] The macroscopic mechanical properties also seem to be strongly influenced by the nanofibrillar arrangement of sequences of crystalline blocks and short-range ordered polymeric chains.[13] Theoretical mechanical models of silks have already been proposed using different approaches. Thus, Termonia[14] discusses the crystallites in terms of multifunctional cross-links with considerable analogy to carbon black in synthesized elastomers. Porter et al.[11] apply mean-field theory to predict macroscopic stress−strain curves from molecular properties. Gersappe[15] reports on molecular dynamics simulations and finds that the mobility of nanoscopic filler particles can control the ability to dissipate energy in polymer nanocomposites. Zhou et al.[16] interpret the properties of spider silk in terms of a hierarchical chain model which gradually unfolds upon stretching the fiber. Remarkably, an experimental study on the thermoelasticity of wet spider silk fibers[17] suggests that the amorphous regions act like rubber and exhibit an entropy elasticity. This observation may also be in accordance with most of the theoretical approaches. For a polymer exhibiting entropy elasticity, the resistance to an externally applied force is a consequence of the decrease of entropy in the system upon extension, while the intermolecular potentials remain unaffected.

With this article, we report on a complementary experimental study to address the question how the mechanical properties of dry silkworm silk are governed by the amorphous regions and whether they can be explained by a model related to entropy elasticity. This central question translates into the experimentally accessible question whether or not an externally induced strain has a measurable effect on chemical bonds in the amorphous regions. The absence of such an effect would be an argument for the model of entropy elasticity even in dry silk.

An adequate method to address this question by probing the predominant hydrogen bonds in silk fibers is provided by neutron time-of-flight spectroscopy. This method gives informa-

* Corresponding author. E-mail: seydel@ill.fr.
† Institut Laue-Langevin.
‡ IEAP, University of Kiel.

10.1021/ma0624189 CCC: $37.00
Published on Web 01/26/2007

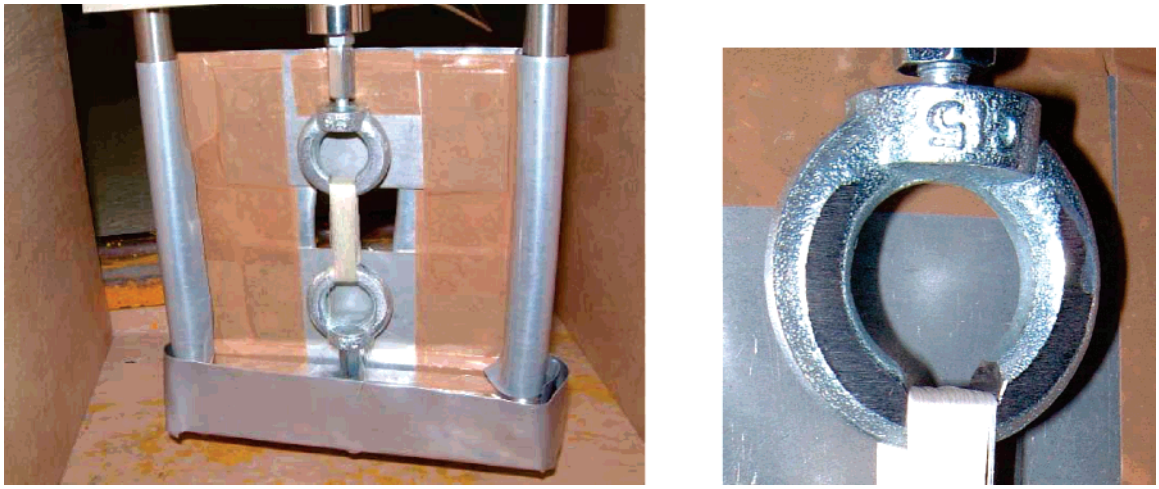

Figure 1. Photographs of a sample mounted on the tensile machine used for neutron spectroscopy (left) and of one of the steel hooks carrying the sample (right). The silk fibers were wound on specially adapted steel hooks with a flat section on the inner bottom side to evenly distribute the force to all fibers. The hooks were attached to a computer-controlled stress−strain device (tensile machine) allowing for a maximum force of 2500 N.[22] Highly aligned fiber bundles were obtained. The fiber axis was vertical and thus perpendicular to the horizontal scattering plane of IN6. Only about 60% of the total mass of the sample was illuminated by the beam, the remainder was shielded by the cadmium mask upstream of the hooks and around the rods of the stress−strain device (seen in the photo from the rear, i.e., downstream side). The samples were each made up of no more than two or three uninterrupted strings of silk.

tion on vibrational modes in the millielectronvolt energy transfer range. Thus, while most other spectroscopic techniques are restricted to the center of the Brillouin zone, neutron spectroscopy probes microscopic dynamics as a function of length scale. In addition, a diffraction pattern is recorded in situ and visualizes any structural changes as a function of tensile strain. The assignment of detectable motions to corresponding structures is of special value in samples with the complexity of biological material. Further, neutron spectroscopy can be enhanced by a selective deuteration of the samples and thus applying contrast variation techniques. In the particular case of silks, predominantly only the amorphous regions are accessible to guest molecules like water.[3] A residual deuteration is possible by immersing the samples in heavy water and a subsequent drying process.[18] Adding to the advantages, cold or thermal neutrons have energies of the order of a few millielectronvolts and hence do not induce any noticeable beam damage due to ionization in biological samples.

In order to apply the neutron spectroscopy technique, however, considerable technical challenges have to be met. Even at the high-flux time-of-flight spectrometer IN6 at the research reactor of the Institut Laue-Langevin, sample masses of more than 100 mg are required for inelastic spectroscopy on biological material. This already requires considerable tensile forces of the order of 1 kN, which have to be applied in situ to the silk fiber bundle to reach the region of plastic deformation. It is furthermore required for our study to adjust the tensile force to the fibers and to record stress−strain curves in situ while recording the neutron inelastic scattering spectra.

Recently, we have established the feasibility of such a type of experiment, and in this article we also report on the technical solutions found within the extended experimental section. We have carried out the experiments using *Bombyx mori* silkworm silk. The tensile strength of *B. mori* (about 500 MPa[19]) is smaller by a factor of approximately two than the strength of spider dragline silk. However, silkworm silk can be obtained more easily in large quantities. We note that *B. mori* silk is more crystalline (about 60% crystallinity[20]) than spider dragline silk. The extensibility is lower for silkworm silk than for spider dragline silk.

The neutron spectroscopy experiment has been complemented by in situ synchrotron X-ray diffraction measurements on *B. mori* silk fiber bundles upon tensile strain. The X-ray experiment provides information on the structural changes in the silk fiber upon the externally applied strain. In particular, the morphological changes in the crystalline regions can thus be quantified with a high accuracy, and indirect conclusions on the disordered regions can be drawn.

In the following sections, we describe the experimental setup for both the neutron and synchrotron experiment in detail and subsequently present and discuss the results. Tentative conclusions and an outlook are provided in the last section.

2. Experimental Section

Samples. We have obtained degummed silkworm silk from the "Musée de la soie", F-30170 St-Hippolyte-du-Fort, France. The degumming was done by unreeling the silk in warm water containing soap. This degumming process aimed at removing the sericine layer on the silk fibers is known to be not entirely efficient. Thus, small quantities of residual sericine may be assumed to be present on the fibers used. In addition, we note that this traditional method of degumming may induce damage to the silk protein.[21] All experiments described in this article have been carried out using fibers from the same batch of silkworm silk. The silk samples, as obtained, consist of twisted double fibers. One individual fiber in turn consists of several subfibers (called brins) and will therefore hereafter be denoted as a "strand bundle". The diameter of the strand bundles was measured using image processing software on digitized optical micrographs. Each strand bundle of (47 ± 3.5) μm in diameter and, thus, of a total cross section of (1735 ± 258) μm ^{2} is composed out of individual brins of ≈10 μm in diameter. Each strand bundle consists of 20 such brins. Thus, assuming a dense packing (factor 0.9) of the brins in the strand bundles, an effective cross section of (1562 ± 232) μm^2 is obtained (corresponding to 20 individual brins), which was used for the calculation of stress from the measured force in the tensile test experiments described below. All stress values thus have the same systematic error of about 15%, however, values from different experiments are directly comparable.

Neutron Spectroscopy. The fibers were wound on specially adapted steel hooks attached to a computer-controlled stress−strain device allowing for a maximum force of 2500 N[22] (Figure 1). The force was measured in situ with an Entran ELPM-T3M-2.5kN-/

L3N sensor mounted between the upper steel hook and the movable upper center rod which sets the force. Highly aligned fiber bundles were obtained. The samples were each made up of no more than two or three uninterrupted strings of silk. In situ deuteration and, when applicable, subsequent reprotonation, was done by immersing the samples in situ for at least 20 min in D_2O or H_2O, respectively, and subsequent drying in vacuum monitored by a pressure gauge and the neutron spectra themselves. By this procedure, it was made sure that the sample alignment and amount of sample in the beam would not be affected as demonstrated in the case of cellulose before.[18] The samples were always kept under vacuum (pressure $\approx 10^{-4}$ mbar) at ambient temperature during the data acquisition.

The experiments were carried out at the cold neutron time-of-flight spectrometer IN6 at the high-flux reactor of the Institut Laue-Langevin (ILL) in Grenoble, France. The incident neutron wavelength was selected by a set of three graphite monochromators and kept always fixed at $\lambda = 5.1$ Å. The energy resolution in this configuration was approximately 70 μeV fwhm. The incoming neutron beam size was defined by cadmium slits and amounted to approximately 20 × 30 mm^2 (width × height). A total of 337 elliptical ^{3}He detectors at a sample-to-detector distance of 2.48 m cover an angular range from 10 to 115° in the horizontal scattering plane and a vertical angular range of ±15°. Vertically, the detector tubes are grouped in three parallel rows, one row being centered in the scattering plane (middle row with 123 detectors), one row above (top row with 107 detectors), and one row below (bottom row with 107 detectors).

During the neutron spectroscopy experiment reported in this article (ILL experiment no. 8-02-326), the silk fiber axis was always vertical, and two different samples, namely sample v1 with the mass $m_{v1} = 288.8 \pm 1.5$ mg and sample v2 with $m_{v2} = 342.7 \pm 1.5$ mg, were used. Only about 60% of this mass was illuminated by the neutron beam, while the remainder was shielded by the cadmium mask around the hooks and rods of the tensile machine. The maximum change in the height of the gap between the steel hooks supporting the fibers upon stretching did not exceed 2 mm. This change of gap has to be taken into account for a proper normalization of the scattering signal as it changes the amount of the sample illuminated by the beam (see section 3). We note that for the change of the gap, only the upper steel hook moves, while the lower hook is fixed to the frame of the tensile machine. The cross sections of the two samples v1 and v2 were determined by comparing the sample mass with that of 32 double fiber strand bundles cut out of the sample after the experiment, 14.9 ± 0.1 mg. Thus, sample v1 contains 1472 ± 7 single fiber strands, sample v2 1240 ± 7. The samples on the steel hooks resemble to a double-layered sheet with a gap defined by the width of the hooks. The corresponding fiber cross sections thus have to be multiplied by a factor of 2 to account for the two sheets. Therefore, the total cross sections of the two samples are 4.598 ± 0.022 and 3.874 ± 0.022 mm^2, respectively. The total flight path from the sample to the detectors is 2.48 m, and the time-of-flight acquisition channel width is approximately 10 μs, while the neutron velocity v at $\lambda = 5.1$ Å is $v = 776.1$ m/s. The gap with a width between the two fiber sheets of approximately 7.5 mm and the width of each sheet of approximately 10 mm thus have a negligible effect on the time-of-flight spectra (as they correspond to just approximately one channel width) and the radial width of the diffraction peaks (as the relative error in the detection angle due to the spatial sample extension is smaller than 10^{-3}). However, the sample geometry induces an anisotropy in the scattering and absorption probability which has not been corrected for. The fiber sheet plane was parallel to the plane defined by the two supporting rods of the tensile machine (see Figure 1), and this plane was aligned such that the shade from the rod pointing to the highest scattering angle was just above the highest detectable scattering angle. The acquisition time per neutron spectrum is typically between 2 and 4 h. The diffraction patterns extracted from the neutron spectra have been corrected for the different counting efficiencies of the individual detector tubes by normalizing to the scattering signal of a vanadium sample. This vanadium sample was measured in a cryostat at $T < 130$ K during the same reactor cycle, but not during the same experimental run, and therefore small inaccuracies may be induced by this normalization. In addition, inaccuracies may be induced by geometrical effects for instance caused by an anisotropic absorption. The analysis and visualization of the neutron data was done using MATLAB.

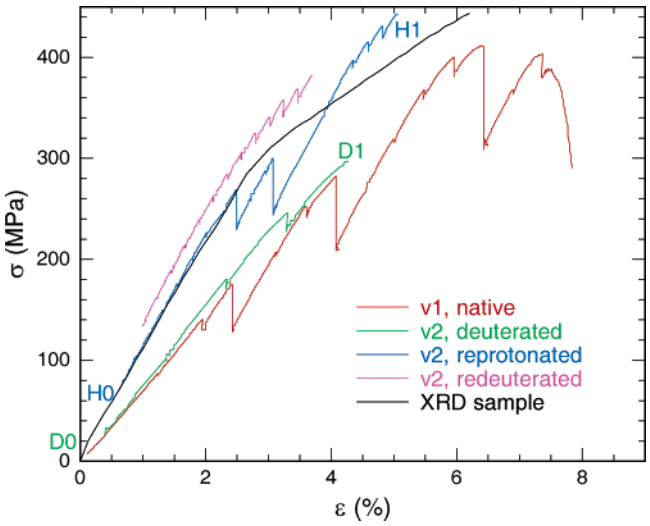

Figure 2. Stress (tensile force per cross section area) σ of the *B. mori* silk fiber bundles measured in situ during the neutron scattering experiments at ILL beamline IN6 plotted vs the strain (relative elongation) ϵ. All stress−strain curves recorded during the neutron spectroscopy experiment are shown. The v1 and v2 in the legend indicate the corresponding sample. The stress strain curves have been measured in the order of the legend from top to bottom. The symbols H0, H1, D0, and D1 mark the positions in the stress−strain history where the spectra depicted in Figure 6 have been recorded. For comparison, the stress−strain curve of the X-ray diffraction experiment (XRD sample) on three double strand bundles is displayed as well.

X-ray Diffraction. Double strand bundles of silk were carefully extracted with the help of tweezers. Three double strand bundles were glued with cyanoacrylate glue (superglue) across the opening of a small paper frame. The initial free fiber length was 4.03 ± 0.08 mm (measured in the same way as the cross section; see above). Tensile tests were carried out using a computer−controlled tensile testing machine designed for a maximum force of 5 N.[23] The paper frame was clamped into a specially designed transfer holder. Already there, the two sides of the paper frame could be cut, as the holder serves the purpose of protecting the fibers from being strained during transfer into the machine and before the start of the tensile test experiment. The force was measured with an Entran SA force sensor ELG-H-5N-/Z2L2M, length changes with a high−precision length gauge (Dr. Johannes Heidenhain GmbH). The fibers were continuously stretched at a rate of 1 μm/s, corresponding to about 1.5%/min.

The in situ X−ray scattering experiments were carried out using synchrotron radiation with a wavelength of $\lambda = 1.5$ Å at the beamline A2, HASYLAB (DESY, Hamburg, Germany). We used a 250 μm × 250 μm cross section of the focused X−ray beam provided by a pair of microslits. Background was reduced by additional guard slits in front of the sample and a small lead beam stop placed immediately behind the exit window of the stretching device. The sample−to−detector distance was 72.1 mm. Fiber diffraction patterns were recorded with a Photonics Science GemStar−2 HS image−intensified CCD detector. Diffraction images were taken during the continuous stretching experiment. Exposure time was 10 s, the time between two images was 1 s. The inset of Figure 3 shows an average of 23 background-subtracted diffraction diagrams.

In order to maximize the intensity of the silk meridional 002 reflection (indexed according to[12]), the sample was tilted by the 002 Bragg angle of 9° with respect to the incident beam.[24] The *d*-spacing of this reflection as a measure of strain in the nanocrystals was obtained using the calibration, integration and fitting routines

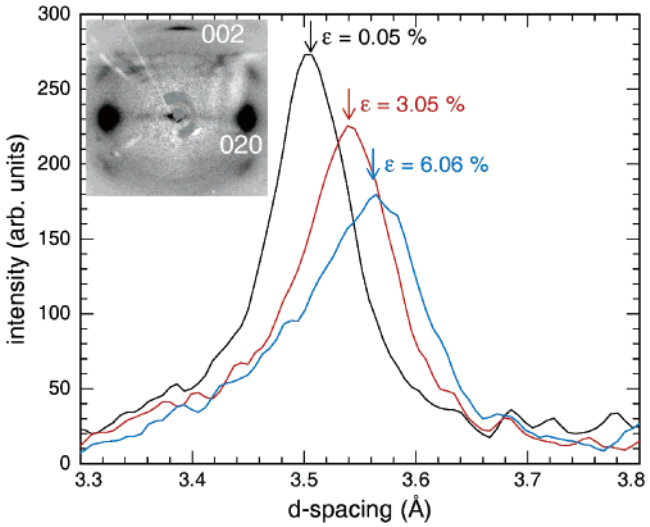

Figure 3. Results from the X-ray diffraction experiments on Bombyx silk fibers at the HASYLAB beamline A2. The inset shows the average of all 23 two-dimensional diffraction patterns recorded after background subtraction. The inhomogeneity of the remaining background is due to the saturation in the center of the diffraction diagram, to a different shading of parts of the detector at different strain, and to the glass capillary of the beamstop holder (diagonal line to the center). The sample was tilted by the Bragg angle of the clearly visible meridional 002 reflection (indexed according to ref 12). The two strong reflections on the equator are indexed 020, and the four equivalent weaker reflections are indexed 021. An azimuthal integration of the 002 reflection at different strain ϵ leads to the curves in the main figure. The expansion of the unit cell with increasing strain in the direction of the *c*-axis is well visible.

of the ESRF software *fit2d*.[25] Three example curves are displayed in Figure 3.

3. Results and Discussion

Stress—Strain Curves Recorded in Situ. During both the X-ray and neutron scattering experiments, the externally applied force was measured in situ while the samples were mounted on the respective scattering instrument (Figure 2). Thus, the diffraction patterns and spectra recorded at different forces and—in the case of neutron spectra—different deuteration states can be directly compared. The curve marked "XRD sample" will be discussed first as with only three individual double strand bundles, bundle effects are minimal for this sample. The bend (yield point) at about 2.8% strain is characteristic of silk; the yield stress of 300 MPa compares well with values from the literature (see, e.g., ref 24). The ultimate stress was not determined in this experiment as the experiment was stopped at $\sigma = 450$ MPa. The initial Young's modulus is 10.7 ± 1.6 GPa, at the upper end of values found in the literature (discussion in ref 24).

Whereas in the X−ray diffraction experiment a constant strain rate was employed, the stretching had to be stopped for the acquisition of neutron time-of-flight spectra. Since silk—like most biological materials—is viscoelastic, the relaxation is visible as a vertical line in the stress−strain curves of samples v1 and v2. Before the start of the measurement, we waited for a few minutes for the fast relaxation on this time scale to finish. The points on the stress−strain curves where measurements were taken are marked in Figure 2. H0: (re-)protonated, $F =$ 200 N. H1: (re-)protonated, $F = 1600$ N. D0: deuterated, $F =$ 0 N. D1: deuterated, $F = 950$ N.

Generally, the bundle stress−strain curves exhibit very similar slopes. An influence of the stretching history of the fibers is visible: fibers stretched for the second and third time (v2 reprotonated, v2 redeuterated) have a higher initial Young's modulus.

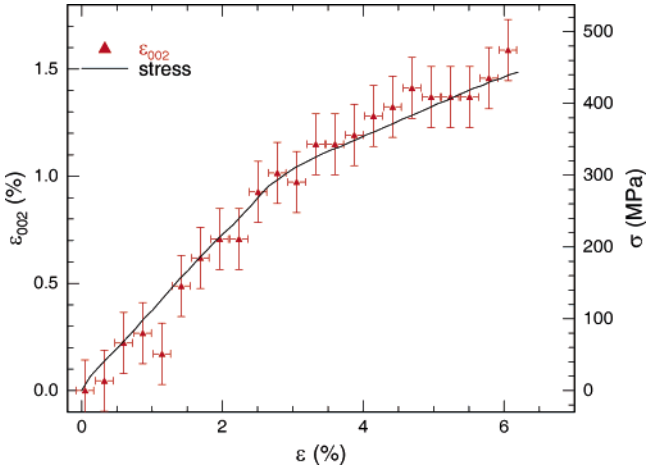

Figure 4. Crystal strain (ϵ_{002}) (symbols, left *y*-axis) within Bombyx silk fibers as extracted from the synchrotron X-ray diffraction data (Figure 3) and stress σ (line, right *y*-axis, same as the black line in Figure 2) measured in situ during this experiment, plotted vs the measured strain ϵ of the fiber.

X-ray Diffraction. The stress−strain curve of three double strand bundles of *B. mori* silk is repeated in Figure 4 (black line, right scale). The red triangles in Figure 4 (left scale) denote the crystal strains ϵ_{002} in the direction of the crystallographic *c*-axis; this axis is parallel to the macroscopic fiber axis. The ϵ_{002} values were calculated from the *d*-spacings of the meridional 002 reflection (see Figure 3) according to $\epsilon_{002}(\epsilon) = (d_{002}(\epsilon) - d_{002}(0))/d_{002}(0)$ with the macroscopic (fiber) strain ϵ. With the appropriate scaling and within the error bars, ϵ_{002} follows the stress−strain curve exactly. In other words, external stress σ and the microscopic crystal strain are proportional, indicating a homogeneous stress distribution in the silk fibers across amorphous and crystalline regions. The ratio between crystal strain and macroscopic strain is about four. Thus, whereas the nanocrystals carry a significant part of the external load, the amorphous regions have to account for most of the elongation of the material.

The most likely scenario in the view of these new results is that the current model for spider silk[14] also applies to the chemically similar silkworm silk: the amorphous polypeptide molecules form a disordered, entangled network at zero strain. Their extension does not need as high stress as a stretching of the crystals, because their first reaction to tensile stress will not be a stretching of the whole polymer chain but rather a straightening of the molecules. The amorphous regions are thus shown to be of major importance for the mechanical properties of the biological nanocomposite silk and were studied further by inelastic neutron scattering and in situ neutron diffraction.

Neutron Scattering: Data Acquisition and Normalization to the Total Scattering. Although the general considerations concerning the data acquisition on the neutron spectrometer IN6 and the data normalization are somewhat straightforward, we nevertheless report them here in detail, because this allows to better estimate the accuracy of our results.

From the neutron scattering intensity $I(\theta, \phi, \text{tof})$ recorded on IN6 as a function of the in-plane scattering angle θ, the azimuth scattering angle ϕ, and the time-of-flight channel tof, both angle-integrated time-of-flight spectra and diffraction patterns can be extracted as follows:

$$I(\phi, \text{tof}) = \sum_{\theta} I(\theta, \phi, \text{tof}) \quad \text{(time-of-flight spectrum)} \qquad (1)$$

$$I(\theta, \phi) = \sum_{\text{tof}} I(\theta, \phi, \text{tof}) \quad \text{(diffraction pattern)} \qquad (2)$$

where the azimuth angle ϕ only takes three discrete values corresponding to the top, middle and bottom detector rows, and the sums are over all available channels in the respective variable.

The recorded intensities have been normalized to the incident beam monitor and subsequently to the total scattering of the sample, as follows: For each recorded spectrum, all intensities were summed over all 337 detectors of the three detector banks of the spectrometer and all time-of-flight channels, yielding an individual scalar value $I_{\text{total},e}$ with $e \in \{\text{H0, H1, D0, D1}\}$ for each spectrum:

$$I_{\text{total},e} = \sum_{\theta,\phi,\text{tof}} I_e(\theta, \phi, \text{tof}) \quad \text{(normalization constant)} \quad (3)$$

In addition, the analog total intensity $I_{\text{total,initial}}$ prior to the deuteration at zero strain for the same sample has been obtained. The monitor-normalized intensities $I_e(\theta, \phi, \text{tof})$ with $e \in \{\text{H0, H1, D0, D1}\}$ of the diffraction patterns have thus been corrected for the change in the total scattering due to the different extension of the fiber bundle to obtain $I_{e,\text{corr.}}(\theta, \phi, \text{tof})$ according to the following equations:

$$I_{\text{H0,corr.}}(\theta, \phi, \text{tof}) = I_{\text{H0}}(\theta, \phi, \text{tof})/I_{\text{total,H0}}$$

$$I_{\text{H1,corr.}}(\theta, \phi, \text{tof}) = I_{\text{H1}}(\theta, \phi, \text{tof})/I_{\text{total,H1}}$$

$$I_{D0,\text{corr.}}(\theta, \phi, \text{tof}) = I_{D0}(\theta, \phi, \text{tof})/I_{\text{total,initial}}$$

$$I_{\text{D1,corr.}}(\theta, \phi, \text{tof}) = I_{\text{D1}}(\theta, \phi, \text{tof})/I_{\text{total,initial}} \times I_{\text{total,D0}}/I_{\text{total,D1}} \quad (4)$$

Please note that the last two equations have been used to take into account the fact that the total scattering volume also changes due to the deuteration of the sample. We have obtained the following ratios: $I_{\text{total,H0}}/I_{\text{total,H1}} = 1.0272$, $I_{\text{total,D0}}/I_{\text{total,D1}} = 1.0131$, $I_{\text{total,initial}}/I_{\text{total,H0}} = 1.0134$, and $I_{\text{total,D0}}/I_{\text{total,initial}} = 0.9275$. The reason for correcting the deuterated spectra with $I_{\text{total,initial}}$ rather than $I_{\text{total,H0}}$ is that the deuterated spectra were recorded before the protonated spectra in the stress−strain history (Figure 2).

In Situ Neutron Diffraction. The neutron diffraction patterns (Figure 5) contained in the neutron spectral information recorded on the instrument IN6 (Figure 6) will be discussed prior to the time-of-flight spectra, as the diffraction patterns also illustrate the effects of the deuteration and the tensile strain on the total scattering of the sample. The diffraction information (Figure 5) has been obtained according to eq 2 and normalized according to the set of equations—eq 4. Since the detector efficiency is not identical for all detectors, the individual detector intensities have been approximately corrected by the scattering from a vanadium normalization sample (see section 2).

In Figure 5, the diffraction patterns are given for the upper detector row (Figure 5 (a)) and the middle detector row (Figure 5c) for the deuterated sample v2 (D0 and D1) and the reprotonated sample v2 (H0 and H1) recorded at the positions in the stress−strain history marked correspondingly in Figure 2. The diffraction patterns recorded in the lower detector row

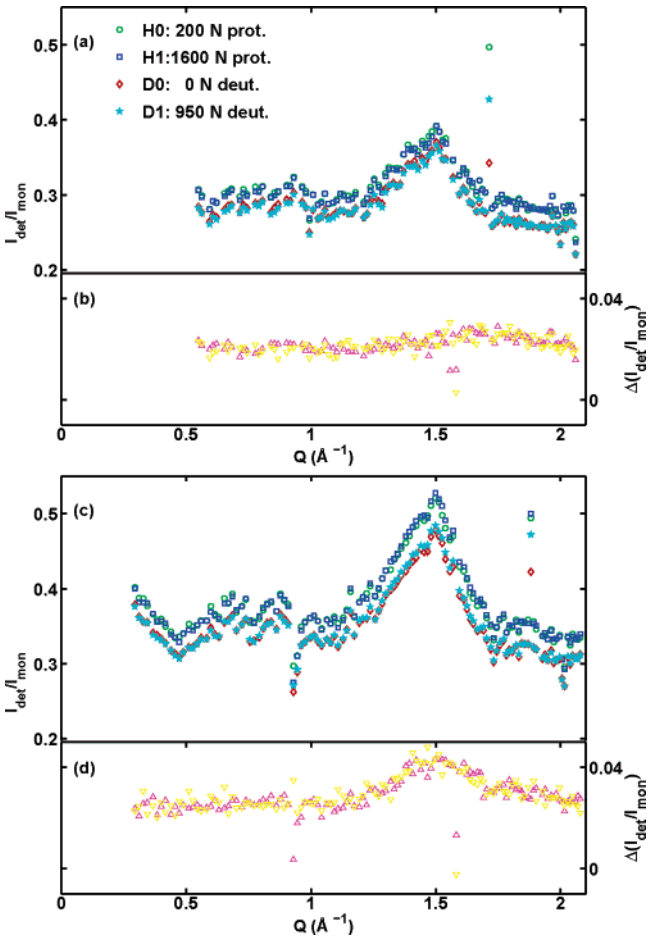

Figure 5. Diffraction patterns of *B. mori* silk fibers obtained from the data recorded on IN6 according to eq 2, normalized to the incident beam monitor and to the total scattering according to the set of eqs 4, and approximately corrected for the individual detector efficiencies by vanadium scattering. The data are plotted vs the absolute value of the total scattering vector Q. The lowest four detectors have been omitted. (a) Data recorded in the top detector row (inclined by 15° with respect to the equatorial plane). (b) Difference patterns from the protonated and deuterated sample for the top detector bank (Δ symbols, H1−D1; ∇ symbols, H0−D0). (c) Data recorded in the equatorial plane of the fibers (middle detector row). The caption of part a applies to part c as well. (d) Difference patterns from the protonated and deuterated sample for the middle detector bank (Δ symbols, H1−D1; ∇ symbols, H0−D0).

are similar to those recorded in the upper detector row and therefore not shown.

In the diffraction patterns thus obtained and depicted in Figure 5, parts a and c, the 020 reflection from the crystallites in the silk can be clearly identified above the incoherent scattering background near $Q = 1.5$ Å^{-1}. This peak is most pronounced in the middle detector row. The peak maximum-to-background ratio is approximately equal for the protonated and deuterated patterns, while the total scattering is lower for the deuterated spectra. This indicates that an H/D-exchange takes place, reducing the total scattering signal. In the middle detector row (Figure 5c), the peak intensity seems to rise slightly upon extension of the fiber. This very small effect could indicate an alignment effect of the fibers as a whole or of the crystallites due to the strain.

The difference spectra from the protonated and deuterated patterns are given in Figure 5, parts b and d for the top and middle detector row, respectively. A weak peak remains in the difference spectra between the patterns from the protonated and deuterated samples, which is most pronounced for the middle

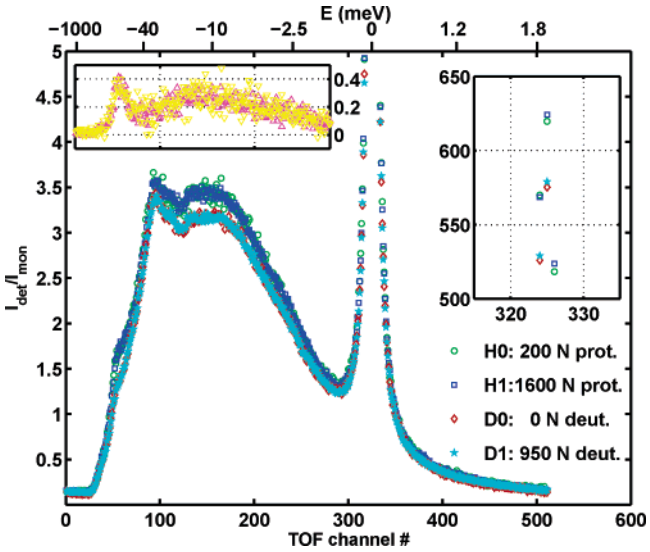

Figure 6. Time-of-flight spectra of *B. mori* silk recorded on IN6. The intensities recorded in all detectors within the equatorial plane have been summed up. The intensities are normalized to the incident beam monitor and corrected for the change in the total illuminated sample volume due to the different extension upon the externally applied stress (see main text for further explanation). The data are plotted vs the time-of-flight channel number. The corresponding calculated energy transfer is indicated in the additional top *x*-axis. The elastic peak maxima are plotted in the right inset using the same axis units as in the main figure. The legend assigns the symbols for both the main part of the figure and the right inset. The difference spectra from the protonated and deuterated sample are given in the left inset. Here, the time-of-flight and energy axis are identical to the corresponding axes of the main part of the figure, and the Δ symbols correspond to the difference between the protonated sample at 1600 N and the deuterated sample at 950 N (H1−D1), while the ∇ symbols denote the difference between the protonated sample at 200 N and the deuterated sample at 0 N (H0−D0).

row. It is known from wide angle diffraction for the similar case of spider silk that no H/D exchange takes place in the poly(alanine) β-sheet crystallites.[3] The observation in the difference patterns depicted in Figure 5, parts b and d, may be in agreement with this observation, because a partial H/D exchange in the amorphous regions may enhance the scattering contrast between crystalline and amorphous regions. It is also possible that an H/D exchange corresponding to a similar correlation length takes place in the amorphous regions of the fiber. Please note that differences of diffraction patterns from protonated and partially deuterated samples have to be interpreted with due care since the proton has a negative coherent scattering length, while deuterium has a positive one.

Neutron Spectroscopy. Time-of-flight spectra recorded on the instrument IN6 are depicted in Figure 6. Here, the intensities recorded in the detectors within the horizontal scattering plane, i.e., the equatorial plane of the fibers, have been integrated to enhance the counting statistics at the expense of the wavevector information according to eq 1. All spectra shown in Figure 6 have been recorded using sample v2, according to the positions in the stress−strain curve marked D0, D1, H0, and H1 in Figure 2. The neutron spectra have been obtained from the same data sets as the corresponding diffraction patterns discussed above along with Figure 5 and normalized according to the set of eqs 4. Unlike in the case of the diffraction patterns, no detector efficiency correction by a vanadium scattering signal has been carried out for the time-of-flight spectra.

The immediate observation provided by Figure 6 is that the vibrational spectra recorded on the deuterated silk (denoted D0, D1) are significantly different from the spectra on the protonated sample (denoted H0, H1). In contrast, there is no noticeable difference between the corresponding spectra at different applied forces (i.e., H0 vs H1 and D0 vs D1, respectively). The example spectra illustrate the situation for a very low or zero force, and a large force clearly above the yield point of plastic deformation, for both the protonated and deuterated sample, respectively. The spectra taken at intermediate forces (not shown) are in agreement with the immediate observation. Thus, there is no noticeable difference in the molecular vibrational response of the silk fibers within the energy range accessible by IN6.

The spectra depicted in Figure 6 also include the elastic line, i.e., the scattering at zero energy transfer $E = 0$, arising from immobile scatterers in the sample (the right inset of the figure). The only noticeable difference in the elastic scattering of the different spectra arises from the different total scattering cross sections of the protonated and deuterated sample, respectively. The spectrometer response to the elastic scattering is the instrumental resolution function with a width of $\approx$70 μeV fwhm. This width is not noticeably broadened by any so-called quasi-elastic scattering from the silk samples. Thus, the absence of any relaxation or diffusion motion in the—notably—vacuum-dry silk can be concluded from our data within the instrumental resolution. There is also no noticeable effect in the wavevector dependence of the elastic peak maximum upon the applied strain (not shown). Thus, there is no change in the mean squared displacement of the scatterers in the sample within the experimental resolution.

The difference spectra from the protonated and deuterated sample for the cases of the (nearly) zero and the large applied force are given in the left inset of Figure 6. The *x*-axis of this inset is identical to the *x*-axis of the main part of the figure. The inset confirms the immediate observation of the complete absence of an effect of the applied strain. Because of the low-energy resolution at high-energy transfers, it is difficult to precisely assign the peak in the difference spectra with a maximum near $E = -79$ μeV. It may tentatively be assigned to the H/D exchange in the amide groups of the accessible amino acids by comparing with infrared spectra.[4] We also refer to related work on nylon fibers using filter−analyzer neutron spectroscopy.[26] Since in analogy to spider silk[3] probably only the amorphous regions within the silk are accessible to water, we assume that the H/D exchange visible in the spectra is due to the H/D exchange in amino acids with exchangeable protons which are present in the amorphous regions. An H/D exchange can in principle take place in the amide groups of all accessible amino acids and, when present, in side groups with exchangeable protons specific to some amino acids. (For the amino acid sequence of *B. mori* silk fibroin, see for instance ref 27.) Another argument is that the difference spectra are not structured very much. This is very similar to the case of cellulose where the analog difference spectra have been studied and in addition by inverse deuteration it was proven that only the disordered (i.e., amorphous) regions contribute to the H/D exchange.[18] We can quantify the H/D exchange in our sample as follows, assuming that the H/D exchange does not modify the partial density of states:[18] Let Σ_d be the integral of the difference between the protonated and deuterated spectra in the inelastic region, i.e., the sum over the *y* values of the data points displayed in the left inset of Figure 6. Let Σ_t be the integral over the total inelastic intensity of the protonated sample taken over the same integration range. Then we obtain $\Sigma_d/\Sigma_t = (7.4 \pm 0.5)\%$, which is in good agreement with the value $1 - (I_{\text{total,D0}}/I_{\text{total,initial}}) = 0.0725$ (see the above paragraph on the in situ neutron diffraction). This agreement is reasonable, because $I_{\text{total,D0}}$ and $I_{\text{total,initial}}$ both

correspond to a total scattering at zero strain, in the case of the protonated and deuterated sample, respectively. We note that the value Σ_d/Σ_t obtained for silk is significantly smaller than the H/D exchange observed for cellulose,[18] which amounts to ≈28.5% for amorphous cellulose and to ≈12% for semicrystalline cotton. The smaller value for silk is probably not due to a higher crystallinity but rather to a higher percentage of nonexchangeable hydrogen bound to carbon. The peak visible in the spectra depicted in Figure 6 (main part) with a maximum at $E \approx -30$ meV seems to correspond approximately to a minimum in the difference spectra (left inset of Figure 6). This peak is at present difficult to assign. Since it corresponds to a minimum in the H/D exchange, it may result from a vibrational mode in the crystallites. We note that it also appears in analog time-of-flight-spectra of spider silk.[28]

To complete the presentation and discussion of the results we note that the neutron time-of-flight spectra obtained by summing the top and bottom detector rows of IN6, respectively, (not shown) seem to be equivalent to the spectra from the sum of the middle detector row (Figure 6). The only noticeable difference within the scope of our analysis is a smaller scattering intensity in all the regions (elastic and inelastic) of the top and bottom spectra compared to middle spectra. The elastic peak maximum in the top and bottom banks is thus reduced by a factor of ≈0.77 compared to the elastic scattering detected in the middle row of IN6.

4. Conclusions and Outlook

From our experiments we conclude that the amorphous regions of silk fibers are of major importance for the mechanical properties. In particular, the X−ray diffraction results show that they account for most of the extensibility of silk fibers. By selective deuteration of the water−accessible regions of silk, which we could identify with the amorphous parts, their response to tensile stress was measured with neutron spectroscopy.

According to our results, there is no evidence for a molecular vibrational or reorientational response in the silk fibers upon externally applied stress even beyond the yield point of plastic deformation. Our results are restricted to the energy range accessible by cold neutron time-of-flight spectroscopy. However, since with our neutron spectra we have measured the neutron energy gain due to inelastic scattering in the sample, we can conclude that no thermally excited mode present in the sample is altered due to the strain on the fibers. We note that Raman spectroscopy on silk fibers has revealed significant band shifts at higher energies on the order of more than 100 meV.[29] We assume that these Raman band shifts can be assigned to the crystalline fraction of the silk since Raman spectroscopy does not discriminate between crystalline and amorphous regions in the sample. Please note further that our results are restricted by the experimental geometry where the fiber axis was vertical and the detectors of the spectrometer were near the equatorial plane of the fibers. However, we assume that any effect to molecular mobility along the fiber axis would be reflected by a corresponding effect perpendicular to the fiber axis. We also emphasize that the acquisition time for the neutron spectra is several hours, and therefore we are not sensitive to any immediate effects upon the force applied to the fibers.

Our results may point toward the assumption that the contribution of the amorphous regions of the silk fibers to the mechanical properties can be explained on a thermodynamical basis in terms of entropic elasticity rather than in terms of changing force fields which would affect chemical bonds and molecular motions in the amorphous regions in a measurable way. Of particular interest is the fact that apparently the disordered regions even of dry silk are mobile enough to exhibit such a behavior, which has so far only been described for wet spider silk.[17] The relatively small deformation of the crystalline regions of the silkworm silk fibers (Figure 4) can be assumed to be purely elastic, and the deformation of both the crystalline and amorphous regions contributes to the change of the free energy of the fibers upon tensile strain. We note that the mechanisms leading to the stretching history, i.e., the difference of the stress−strain curves when the fibers are stretched a second and third time from the initial curve (Figure 2), are not fully elaborated yet. The effect may be linked to a breaking of hydrogen bonds upon the initial stretching or to a transition from a glassy to a rubberlike state,[11,14] and it appears that the fibers can return to their initial length after several days. X-ray diffraction experiments as a function of the tensile history of silkworm silk fibers (which are beyond the scope of the present article and will be subject to a separate publication) corroborate the assumption that the crystallites within the silk are elastically deformed when the fibers are stretched. These experiments also indicate that a broad spectrum of relaxation times seems to be present in the stretched fibers, and on a time scale of 10 s, the crystal strain seems to reflect a nonrelaxed stress in the amorphous regions rather than a plastic deformation of the crystallites.

Future studies aimed at enlarging the accessible dynamic range shall give access to molecular mobility in the microelectronvolt energy transfer range using the neutron backscattering technique to probe slow polymer chain motions on nanosecond time scales. Further, the influence of humidity shall be addressed using both X-ray and neutron scattering methods. An even better discrimination of motion in crystalline and amorphous parts of the silk may be achieved by applying polarized neutron scattering techniques.

Acknowledgment. We are grateful to Matthias Elender and Steve Jenkins for technical and engineering support at the ILL and to Martin Dommach and Sérgio S. Funari at HASYLAB. We thank Ingo Grotkopp (University of Kiel) for help with the sample environment for the X-ray diffraction experiment. We are indebted to Daniel Sapede (ILL and ESRF), Christian Riekel (ESRF), and Helmut Schober (ILL) for many stimulating discussions. This work was supported in part by the DFG Grant Nos. MU1673/2-3 and -/3-1.

References and Notes

(1) van Beek, J. D.; Hess, S.; Vollrath, F.; Meier, B. H. *PNAS* **2002**, *99*, 10266.
(2) Simmons, A. H.; Michal, C. A.; Jelinski, L. W. *Science* **1996**, *271*, 84.
(3) Sapede, D.; Seydel, T.; Forsyth, V. T.; Koza, M. M.; Schweins, R.; Vollrath, F.; Riekel, C. *Macromolecules* **2005**, *38*, 8447.
(4) Asakura, T.; Kuzuhara, A.; Tabeta, R.; Saito, H. *Macromolecules* **1985**, *18*, 1841.
(5) Grubb, D. T.; Jelinski, L. W. *Macromolecules* **1997**, *30*, 2860.
(6) van Beek, J. D.; Beaulieu, L.; Schäfer, H.; Demura, M.; Asakura, T.; Meier, B. H. *Nature (London)* **2000**, *405*, 1077.
(7) Hakimi, O.; Knight, D. P.; Knight, M. M.; Grahn, M. F.; Vadgama, P. *Biomacromolecules* **2006**, *7*, 2901.
(8) Shao, Z.; Vollrath, F. *Nature (London)* **2002**, *418*, 741.
(9) Gosline, J. M.; DeMont, M. E.; Denny, M. W. *Endeavour* **1986**, *10*, 37.
(10) Vollrath, F.; Knight, D. *Nature (London)* **2001**, *410*, 541.
(11) Porter, D.; Vollrath, F.; Shao, Z. *Eur. Phys. J. E* **2005**, *16*, 199.
(12) Shen, Y.; Johnson, M. A.; Martin, D. C. *Macromolecules* **1998**, *31*, 8857.
(13) Sinsawat, A.; Putthanarat, S.; Magoshi, Y.; Pachter, R.; Eby, R. K. *Polymer* **2002**, *43*, 1323. Sinsawat, A.; Putthanarat, S.; Magoshi, Y.; Pachter, R.; Eby, R. K. *Polymer* **2003**, *44*, 909.

(14) Termonia, Y. *Macromolecules* **1994**, *27*, 7378.
(15) Gersappe, D. *Phys. Rev. Lett.* **2002**, *89*, 058301.
(16) Zhou, H.; Zhang, Y. *Phys. Rev. Lett.* **2005**, *94*, 028104.
(17) Gosline, J. M.; Denny, M. W.; DeMont, M. E. *Nature (London)* **1984**, *309*, 551.
(18) Müller, M.; Czihak, C.; Schober, H.; Nishiyama, Y.; Vogl, G. *Macromolecules* **2000**, *33*, 1834.
(19) Fossey, S. A.; Kaplan, D. L. In *Polymer Data Handbook*; Mark, J. E., Ed.; Oxford University Press: Oxford, U.K., 1999; pp 970−974.
(20) Freddi, G.; Tsukada, M. In *Polymeric Material Encyclopedia*; Salamone, J. C., Ed.; CRC Press: Boca Raton, FL, 1996; Vol. 10, pp 7734−7744.
(21) Yamada, H.; Nakao, H.; Takasu, Y.; Tsubouchi, K. *Mater. Sci. Eng.: C* **2001**, *14*, 41.
(22) Kölln, K.; Ph.D. Thesis, University of Kiel, Kiel, Germany, 2004 (http://e-diss.uni-kiel.de/diss_1173/).
(23) Grotkopp, I.; Ph.D. Thesis, University of Kiel, Kiel, Germany, 2006 (http://e-diss.uni-kiel.de/diss_1838/).
(24) Sinsawat, A.; Puttharanat, S.; Magoshi, Y.; Pachter, R.; Eby, R. K. *Polymer* **2002**, *43*, 1323.
(25) Hammersley, A.P.; Svensson, S.O.; Thompson, A. *Nucl. Instrum. Methods Phys. Res. A* **1994**, *346*, 312.
(26) Papanek, P.; Fischer, J. E.; Murthy, N. S. *Macromolecules* **2002**, *35*, 4175.
(27) Zhou, C.-Z.; Confalonieri, F.; Jacquet, M.; Perasso, R.; Li, Z.G.; Janin, J. *Proteins—Struct., Funct., Genet.* **2001**, *44*, 119.
(28) Sapede, D.; Ph.D. Thesis, University Joseph Fourier, Grenoble, France, 2006 (http://tel.ccsd.cnrs.fr/tel-00011700?langue=en).
(29) Sirichaisit, J.; Brookes, V. L.; Young, R. J.; Vollrath, F. *Biomacromolecules* **2003**, *4*, 387.

MA0624189